ARTICLE NO. 79-0577R

J80-172

Effects of Inflow Distortion Profiles on Fan Tone Noise

00023
20001
20009

Hiroshi Kobayashi* and John F. Groeneweg†
NASA Lewis Research Center, Cleveland, Ohio

Calculations of the fan tone acoustic power and modal structure generated by complex distortions in axial inflow velocity are presented. The model used treats the rotor as a rotating three-dimensional cascade and calculates the acoustic field from the distortion-produced dipole distribution on the blades including non-compact source effects. Radial and circumferential distortion shapes are synthesized from Fourier-Bessel components representing individual distortion modes. The relation between individual distortion modes and the generated acoustic modes is examined for particular distortion cases. Comparisons between theoretical and experimental results for distortions produced by wakes from upstream radial rods show that the analysis is a good predictor of acoustic power dependence on disturbance strength and fan speed.

Nomenclature

$|a_q|$ = magnitude of the circumferential distortion harmonic
$B_{q,p}$ = Fourier coefficient of inflow distortion
$B_{n,\ell,k}$ = coefficient in series expansion of radial eigenfunction R_n in the terms of R_0, namely

$$R_n(k_{n,\ell}r) = \sum_{k=0}^{L-1} B_{n,\ell,k} R_0(k_{0,k}r)$$

$|b_p|$ = magnitude of the radial distortion harmonic
C_a = axial projection of blade chord length
C_D = drag coefficient of a cylinder
$C_{n,\ell,k}$ = coefficient defined by $C_{n,\ell,k}$

$$= \sum_{m=0}^{L-1} B_{n,\ell,m} \int_h^1 R_0(k_{0,k}\rho) R_0(k_{0,m}\rho)\, d\rho/\rho$$

d^* = diameter of a cylindrical tube or rod
$E^j_\pm$ = dimensionless acoustic power for the jth pure tone harmonic nondimensionalized by $\pi\rho_0 \bar{W}_a^3 \epsilon_a^2 r_T^{*2}/4$
$EI^j_\pm$ = modal component of the dimensionless acoustic power with respect to the jth pure tone harmonic
$F_l(r)$ = radial distortion velocity function defined in Eq. (4)
$G_{0,k}$ = acoustic dipole distribution on the blade surfaces
$\tilde{G}_{0,k}$ = dimensionless acoustic dipole distribution $(=2G_{0,k}/\epsilon_a\rho_0\bar{W}_a^2)$
h = hub-tip ratio
$HP_\pm(n,\ell,q)$ = nondimensional pressure amplitude in the (n,ℓ) acoustic mode
KT_k = upwash kernel function
L = number of terms in the finite series approximation for $G_{0,k}$
L_0 = probe length immersed in duct
M_a = axial flow Mach number
M_T = relative Mach number at the tip
N_B = rotor blade number
N = number of Gaussian profiles
p = radial mode number of inflow distortion
Q = relative flow velocity of undisturbed fluid $(=\bar{W}_a\sqrt{1+\omega_T^2 r^2})$
$q(r,\theta,z)$ = fluctuating velocity
$q_\tau(r,\theta,z)$ = upwash velocity on blade surface induced by dipole distribution
$q_{\tau,w}$ = upwash component of the external fluctuating velocity
q = circumferential mode number of inflow distortion
$R_q(k_{qp}r)$ = radial eigenfunction of q order with eigenvalue $k_{q,p}$
r_T^* = dimensional fan blade tip radius
(r,θ,z) = dimensionless cylindrical coordinate system fixed to the rotor; lengths nondimensionalized by r_T^*
S_0 = pitch-chord ratio
s = dimensionless coordinate along undisturbed streamlines
t = time nondimensionalized by $r_T^*/\bar{W}_a$
(u,v,w) = the (r,θ,z) components of fluctuating velocity
$\bar{W}_a$ = uniform axial velocity
$w_{e,a}$ = axial component of external fluctuating velocity due to inflow distortion
x^* = distance upstream of the rotor blade tip leading edge
$\alpha_\pm$ = axial wave number per length r_T^*, $\alpha_\pm = M_a^2/\beta_a^2 \times (n\omega_T+\omega) \mp |\Omega_{n,\ell}|$
β_a = $\sqrt{1-M_a^2}$
γ = stagger angle
ϵ_a = nondimensional amplitude of the fluctuating velocity $w_{e,a}/\bar{W}_a$
ζ = axial coordinate associated with z
$\Theta_l(\theta)$ = circumferential distortion velocity function defined in Eq. (4)
θ_2 = half-width of the Gaussian circumferential distortion profiles
θ_0 = helical coordinate $(=\theta-\omega_T z)$
ρ_0 = density of undisturbed fluid
σ = interblade phase angle
τ = coordinate normal to r and s
$\Omega_{n,\ell}$ = axial eigenvalues $(=\sqrt{k_{n,\ell}^2-(n+q)^2\omega_T^2 M_a^2/\beta_a^2}/\beta_a)$
ω_T^* = constant angular velocity
ω_T = rotor tip speed/axial flow speed $(=\omega_T^* r_T^*/\bar{W}_a)$
ω = fluctuating frequency on rotor blade due to inflow distortion $(=q\omega_T)$

Presented as Paper 79-0577 at the AIAA 5th Aeroacoustics Conference, Seattle, Wash., March 12-14, 1979; submitted April 25, 1979; revision received Dec. 14, 1979. This paper is declared a work of the U.S. Government and therefore is in the public domain.
Index categories: Aeroacoustics; Nonsteady Aerodynamics; Noise.

*NRC-NASA Research Associate; Senior Engineer, National Aerospace Laboratory, Japan. Member AIAA.
†Head, Turbomachinery Noise Section. Member AIAA.

Superscripts

j	= tone harmonic number
*	= dimensional quantity

Subscripts

k	= radial summation index
ℓ	= radial acoustic mode number
n	= circumferential acoustic mode number
p	= radial inflow distortion mode number
q	= circumferential inflow distortion mode number
+	= downstream propagation
−	= upstream propagation

Introduction

MANY papers have shown that the fan noise level differences between static testing and projections to forward flight are due to the inflow distortion and turbulence present during most static test conditions.[1] However, the importance of the inflow distortion contribution to fan noise will depend on the particular fan stage and inflow distortion structure. It is therefore of interest to theoretically study the fan noise due to inflow distortion interactions with a three-dimensional annular blade row and to compare the results of the theory to existing experimental data. This theoretical study provides the fan noise modal structure which is required for the prediction of far-field radiation patterns[2,3] and the design of acoustic suppressors where inflow distortion is the known source mechanism.[4]

A previous paper[5] presented the three-dimensional theoretical analysis of pure tone fan noise generated by inflow distortion/rotor interaction. It extended the three-dimensional unsteady lifting surface theory developed by Namba,[6] accepted as input various shapes of inflow distortion, and predicted the forward and aft radiated pure tone power and modal power distribution. Special emphasis was placed upon the clarification of the role of the three-dimensional and noncompact source effects. The numerical calculations for the full three-dimensional model, a two-dimensional model, and a quasi-three-dimensional model were carried out and compared for the case of an inflow distortion which was uniform radially and sinusoidal circumferentially. However, real inflow distortions are expected to have more complex shapes than the simple sinusoidal circumferential variation. Therefore, the present paper explores the character of the predicted tone generation for more complex distortion types. In particular, the relation between the modal content of the inflow distortion and the generated acoustic field is emphasized, and comparisons between the theoretical and experimental results for distortions produced by wakes from upstream radial rods are made. In the theoretical procedure, the local inflow distortion is resolved into Fourier-Bessel components, i.e., inlet distortion modes. The effects of each inflow distortion mode are superimposed to obtain the individual acoustic modal powers generated which, in turn, are summed to obtain the total pure tone acoustic power. An important property of this inflow distortion/rotor interaction analysis is that the same acoustic mode can be generated by all the inflow distortion components which have the same circumferential mode number, even though their radial mode numbers are different. The next section summarizes the theoretical model which is described in more detail in Ref. 5.

Analytical Model

Fluctuating Velocity Induced on a Rotor Blade Row

The theoretical model consists of a single three-dimensional annular blade row with N_B blades rotating at constant angular velocity ω_T^* in an annular rigid-walled duct of infinite axial extent, as shown in Fig. 1a. (Note that an asterisk means the quantity is dimensional and lengths are non-

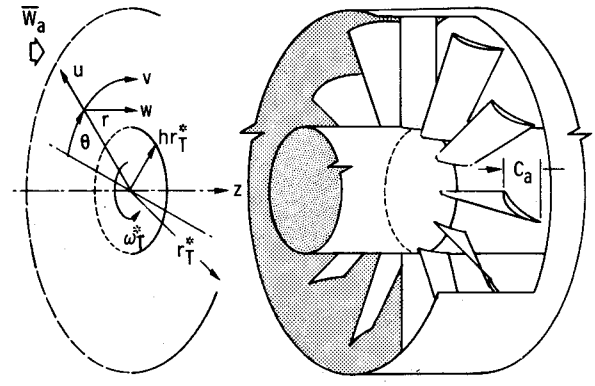

a) FAN GEOMETRY AND COORDINATE SYSTEM.

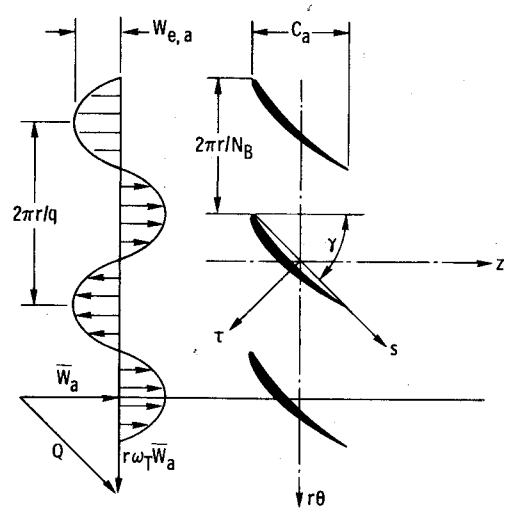

b) INFLOW DISTORTION AND BLADE ROW PARAMETERS AT A CONSTANT RADIUS.

Fig. 1 Nomenclature for analytical model.

dimensionalized by r_T^*, the duct radius.) Thus, the duct end reflection, the effect of upstream and downstream blade rows, and the effects of duct area variation are not considered. But these effects, except for the area variation, could be analyzed using the solution procedure of the present study. The fluid flow (see Fig. 1b) is composed of an undisturbed flow with a uniform axial velocity $\bar{W}_a$ and small fluctuating flows $w_{e,a}$ due to the inflow distortion. The flow is inviscid, of uniform entropy, and has no thermal conductivity. The fluctuations induced on the rotor by the inflow distortion convected by the mean flow are assumed to be isentropic and small compared with the undisturbed flow. It is also assumed that the fluid velocity relative to the blade is subsonic along the whole span and that the blades have no steady load, i.e., a cascade of airfoils which have a helical undisturbed stream-surface $\theta_0 = \theta - \omega_T z$ is analyzed.

The fluctuating velocity $q(r,\theta,z)e^{i\omega t}$ induced by the rotor blade row/distortion interaction can be obtained by integrating the linearized Euler's equation of motion and the upwash component on the blade surface, and can be expressed in the following form:

$$q_\tau(r,\theta,z) = -\frac{1}{\rho_0 Q}\frac{N_B}{4\pi}\sum_{q=-\infty}^{\infty}\sum_{p=-\infty}^{\infty}\int_{-C_a/2}^{C_a/2} \times \sum_{K=0}^{L-1} G_{0,k}(\zeta,q,p)KT_k(r,\theta,z/\zeta,q)\,d\zeta \qquad (1)$$

The detailed expressions for the kernel function KT_k are given in Ref. 5.

Inflow Distortion

In this paper, the inflow distortion is assumed to have only an axial velocity component. (Other components can be considered using the same theoretical methods.) When a Fourier-Bessel analysis of arbitrary shapes of inflow distortion is carried out, the following axial component of external fluctuating velocity is obtained:

$$w_{e,a}(r,\theta,z,t) = \epsilon_a \bar{W}_a \sum_q \sum_p B_{q,p} R_q(k_{q,p} r) e^{-iq(\theta-\omega_T t)} \tag{2}$$

Then, the upwash component of the external fluctuating velocity on a blade surface can be expressed by

$$[q_{T,w}]_{\theta=\omega_T z} = -w_{e,a} e^{-iq\omega_T(z-t)} (\omega_T r/\sqrt{1+\omega_T^2 r^2}) \tag{3}$$

Here, the upwash is defined as the component of disturbed velocity normal to the helical disturbed stream-surface (blade surfaces) placed at $\theta_0 = 0$. It is convenient to suppose that the distortion velocity can be expressed as the product

$$w_{e,a}(r,\Theta)/\epsilon_a \bar{W}_a = F_1(r)\Theta_1(\theta) \tag{4}$$

then,

$$B_{q,p} = a_q \cdot b_p \tag{5}$$

where

$$a_q = \frac{1}{2\pi}\int_0^{2\pi} e^{-iq\theta}\Theta_1(\theta)\,d\theta \tag{6}$$

and

$$b_p = \int_h^1 r \cdot R_q(k_{q,p} r) F_1(r)\,dr \tag{7}$$

When the inflow distortion can be represented by N Gaussian profiles (for $N = 1,2,\ldots$) in the circumferential direction, then

$$\Theta_1(\theta) = \exp\left[\frac{-\left(\frac{\theta}{2\pi} - \frac{1+2j}{2N}\right)^2}{\theta_2^2}\right] \begin{cases} \frac{j}{N}2\pi < \theta < \frac{j+1}{N}2\pi \\ \text{for} \quad j = 0,1,2\ldots,N-1 \end{cases} \tag{8}$$

and we find that

$$a_q = \begin{cases} \sqrt{\pi} N\theta_2 e^{\frac{-i\pi q}{N}} \cdot e^{-\pi^2 q^2 \theta_2^2}\left[Re\ \text{erf}\left(\frac{1}{2N\theta_2} + iq\pi\theta_2\right)\right] \\ 0 \ \text{otherwise for } q = 0,\ \pm N,\ \pm 2N,\ldots \end{cases} \tag{9}$$

Model of Rod Wakes

For the specific case of an axial velocity distortion produced by the wake of a cylindrical tube or rod of diameter d^* the magnitude of the wake defect ϵ_a and the Gaussian half-width of the wake profile θ_2 are given by the following equations based on Prandtl's mixing length hypothesis (cf., Ref. 7, p. 691).

$$\epsilon_a = \frac{1}{4\sqrt{0.0222\pi}}\left(\frac{x^*}{C_D d^*}\right)^{-1/2}\Theta_1(\theta) \tag{10}$$

where $\Theta_1(\theta)$ is given by Eq. (8) and

$$\theta_2 \equiv \frac{0.298}{2\pi r_T^*}\sqrt{C_D d^* x^*} \tag{11}$$

Determination of Acoustic Dipole Distribution

The upwash component of the external fluctuating velocity $q_{T,w}$ must be cancelled by the induced upwash velocity $q_T(r,\theta,z)e^{i\omega t}$ at the blade surfaces. Then, an integral equation for the unknown acoustic dipole $G_{0,k}(\zeta,q,p)$ is obtained in the form

$$\frac{N_B}{8\pi}\left[\int_{-C_a/2}^{C_a/2}\sum_{m=0}^{L-1}\tilde{G}_{0,m}(\zeta,q,p)KT_m(r,\omega_T z, z-\zeta,q)\,d\zeta - B_{q,p}R_q(k_{q,p}r)r\omega_T e^{-iq\omega_T z}\right] = 0 \tag{12}$$

The quantity $\tilde{G}_{0,m}(\zeta,q,p)$ is calculated from Eq. (12) by a collocation method.

Pure Tone Acoustic Power

The dimensionless acoustic power $E^j_{\pm}$ with respect to the jth pure tone fan harmonic (for example, $j = \pm 1$ corresponds to the fundamental) is given by

$$E^j_{\pm} = \sum_q \sum_{n=n_1}^{n2} \sum_{\ell=0}^{\ell_e} EI^j_{\pm}(n,\ell,q) \tag{13}$$

and

$$EI^j_{\pm} = \frac{|HP_{\pm}(n,\ell,q)|^2 \beta_a^2 (n\omega_T+\omega)\,|\Omega_{n,\ell}|}{(\alpha_{\pm}+n\omega_T+\omega)^2} \tag{14}$$

The nondimensional pressure amplitude in the (n,ℓ) acoustic mode is given by

$$HP_{\pm}(n,\ell,p) = -\frac{N_B}{4\pi\beta_a^2}\sum_{k=0}^{L-1}\left[\frac{\omega_T\alpha_{\pm}}{|\Omega_{n,\ell}|}B_{n,\ell,k} - \frac{n}{|\Omega_{n,\ell}|}C_{n,\ell,k}\right] \times \int_{-C_a/2}^{C_a/2}\sum_p \tilde{G}_{0,k}(\zeta,q,p) \times \exp[-i(\alpha_{\pm}+n\omega_T)\zeta]d\zeta \tag{15}$$

For the compact source analysis, $\exp[-i(\alpha_{\pm}+n\omega_T)\zeta] = 1$ in Eq. (15).

Numerical Results

The numerical calculations are carried out in this paper for three different rotor configurations. Their overall geometric and aerodynamic parameters are given in Table 1, and the radial variations of stagger angle γ, pitch-chord ratio S_0, and ratio of blade relative to axial velocity, $Q/\bar{W}_a$ are shown in Fig. 2. The numerical results include four cases: 1) the acoustic power in the modal components generated by particular Fourier-Bessel components of inflow distortion in the case of the fan denoted No. 1; 2) the acoustic power and modal content variations with the half-width of a single Gaussian profile representing the local inflow distortion profile in the circumferential direction (fan 2); 3) the comparison between theoretical and experimental tone power for the case of an upstream distortion produced by the wake of a cylindrical tube immersed to varying depths from the duct wall (fan 2); and 4) the comparison between numerical and experimental tone powers and the analysis of modal content for the cases of 28 and 41 rod wakes interacting with a 28-bladed rotor (fan 3).

Generation by Particular Fourier-Bessel Inflow Distortion Modes

Figures 3 and 4 show the fundamental pure tone modal powers as a function of the circumferential lobe number q of the inflow distortion whose radial distribution is assumed to be the first (Fig. 3) or third (Fig. 4) radial eigenfunction of order q. Figures 3a and 4a are for upstream propagation, while Figs. 3b and 4b are for downstream propagation. The fan used in this calculation has the largest number of blades of the three cases, as shown in Table 1, and, for similar tip speed conditions, generates the largest number of propagating modes. The calculations were limited to $q \leq 50$. The first

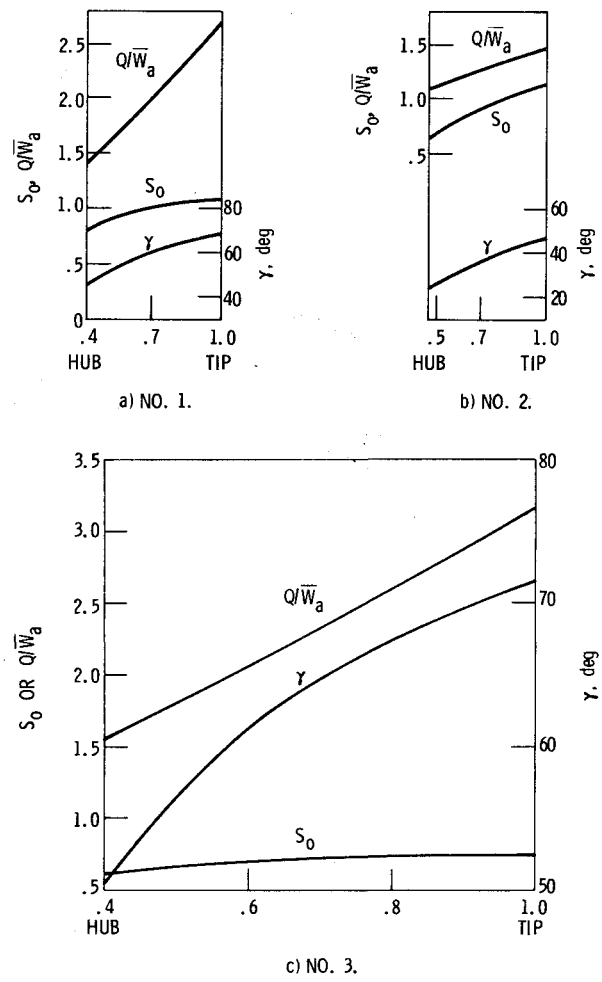

Fig. 2 Radial variations of stagger angle γ, pitch-chord ratio S_0, and velocity ratio $Q/\bar{W}_a$ of the rotor.

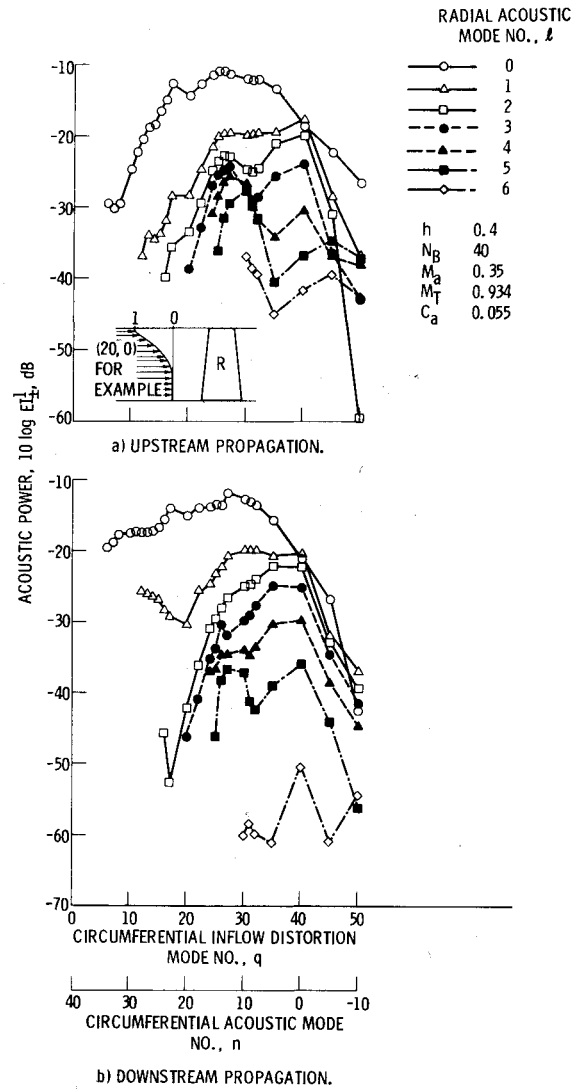

Fig. 3 Fundamental pure tone power variation with radial inflow distortion given by the Fourier-Bessel first radial mode of order q, fan 1, maximum amplitude = 1.

radial inflow distortion mode has a maximum amplitude at the rotor tip, while the third radial inflow distortion mode has peaks near the middle of the blade span. With the radial distortion mode number p held constant, the radial distribution of inflow distortion velocities changes continuously with circumferential distortion mode number q with more skewing toward the wall as q increases. The maximum amplitudes of all inflow distortion modes used in these calculations are equal to 1. The numerical results show that while the first radial mode of inflow distortion generates all radial acoustic modes, the first radial acoustic mode, $\ell=0$, dominates for most values of q. The third radial mode of inflow distortion also generates all radial acoustic modes but, over a wide range of q, many of them carry more power than $p=\ell=2$.

In the case of the first radial mode of inflow distortion (Fig. 3), the first radial acoustic mode power is larger than other radial acoustic mode powers by more than 5 dB in both upstream and downstream cases, except for the points at $q=40$ and the downstream values at $q=50$. At $q=40$, the circumferential inflow distortion mode number equals the rotor blade number, and the circumferential acoustic model number n is zero ($n=jN_B-q$). The (0, 0) acoustic mode is a plane wave. If one accepts the intuitive notion that the acoustic pressure in the various modes will sum in a manner such that the net radial variation will be similar to the radial variation of distortion, then it is reasonable to expect that a combination of second and third radial acoustic modes will exist at $q=40$ in addition to the plane wave. For the cases where $n\neq 0$, the $\ell=0$ modes apparently provide a reasonable radial match to the (q,0) distortion modes.

In the case of the third radial mode of inflow distortion (Fig. 4), the acoustic powers of the higher-order radial modes ($\ell>2$) contribute to the total fundamental tone power over the midrange values of q which correspond to peak total fundamental power generation. The third radial acoustic mode ($\ell=2$) dominates only at lower values of q near 20. Note that the $\ell=2$ acoustic mode in Fig. 4a shows a distinct minimum at $n=10$. This is probably a point where the resultant acoustic dipole distribution on the blades cannot couple with the (10,2) acoustic mode, similar to the case discussed in connection with Fig. 13 of Ref. 9, which applied to rotor-stator interaction. In general, for cases other than the simplest ($p=0$) radial variation of inflow distortion, we are not yet able to rationalize the calculated distribution of radial acoustic mode powers produced by a single higher-order radial distortion mode.

Generation by a Gaussian Circumferential Inflow Distortion Profile

Fan 2 used in this calculation has a low tip speed and small blade number. Therefore, the total number of acoustic modes generated at a particular circumferential distortion mode number is less than for fan 1. Figure 5 shows the acoustic power generated by fan 2 interacting with a single inflow distortion represented by a Gaussian profile in the circumferential direction and a radial step function velocity defect that extends from the blade tip down to 72% of the

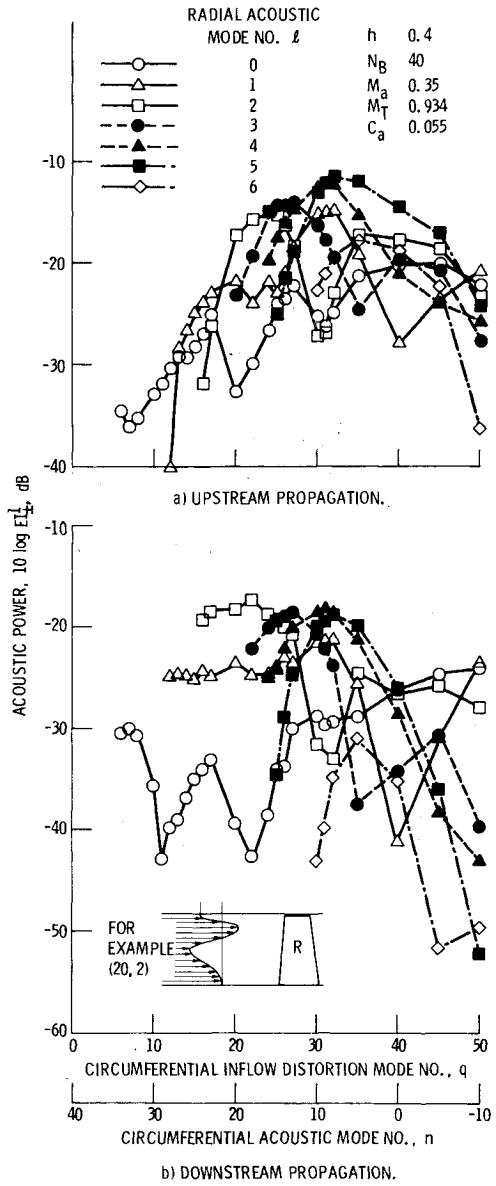

Fig. 4 Fundamental pure tone power variation with radial inflow distortion given by the Fourier-Bessel third radial mode of order q, fan 1, maximum amplitude = 1.

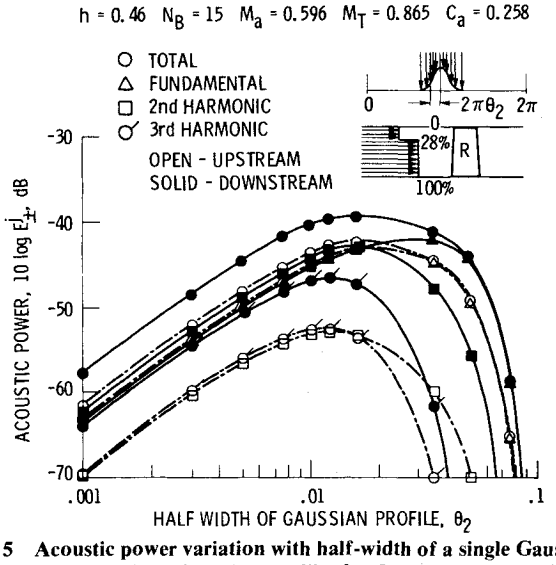

Fig. 5 Acoustic power variation with half-width of a single Gaussian circumferential inflow distortion profile, fan 2, noncompact, 28% tip radial distortion.

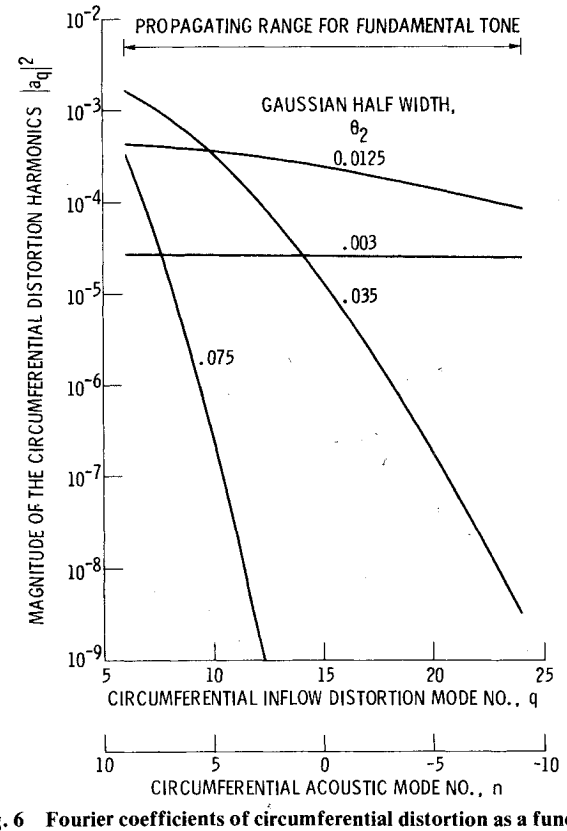

Fig. 6 Fourier coefficients of circumferential distortion as a function of single Gaussian distortion width (fan 2).

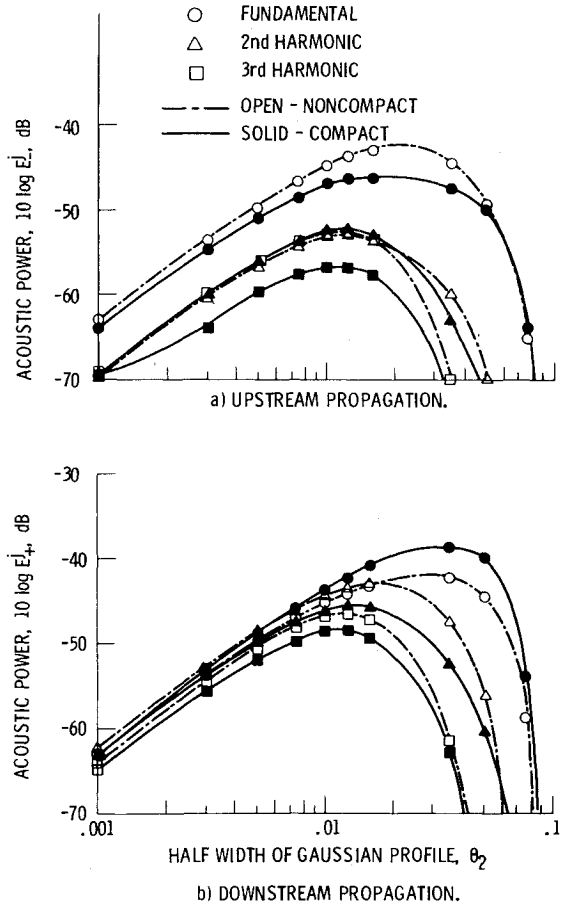

Fig. 7 Comparison of compact and noncompact source acoustic power prediction for a single Gaussian circumferential distortion, fan 2, 28% tip radial distortion.

span. The power is plotted as a function of the half-width of the Gaussian profile θ_2. Results are shown for the total, first, second, and third harmonic tone powers propagating in both upstream and downstream directions.

Figure 5 shows that the acoustic power in any harmonic peaks at particular values of the Gaussian half-width. This phenomenon, mentioned in Ref. 8 and discussed in Ref. 1, is related to an interplay between the number of propagating acoustic modes and the Fourier-Bessel inflow distortion harmonic amplitudes which can couple to the acoustic modes. An example of the circumferential Fourier distortion harmonics corresponding to the conditions of Fig. 5 is shown in Fig. 6 for several values of Gaussian profile half-width. The range of n (or q) corresponding to propagating circumferential acoustic mode numbers is also shown. With an increase in θ_2, the amplitudes of the lower-order circumferential distortion coefficients, $|a_q|^2$, increase; but the large amplitudes occur over a smaller portion of the propagating range. The result of this coupling constraint is a peaking and decline beyond a certain value of profile width.

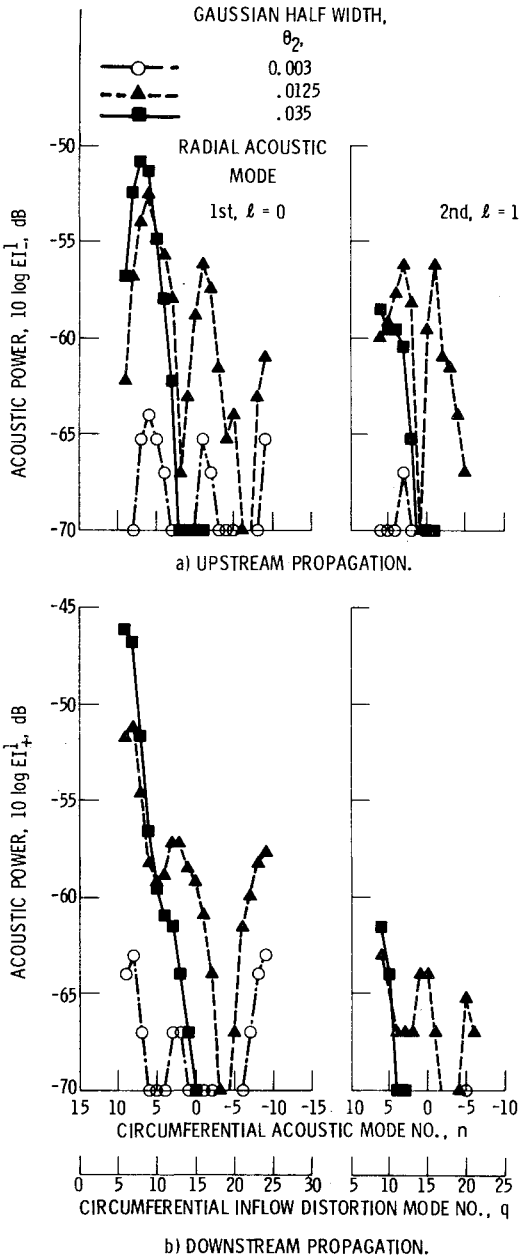

Fig. 8 Variation of the fundamental tone modal structure with half-width of Gaussian circumferential distortion profile, fan 2, 28% tip radial distortion.

For values of θ_2 greater than about 0.02, the downstream propagating acoustic power in the fundamental tone is higher than the upstream power. For the second and third harmonic and the total power, the downstream power is always greater than the upstream power. Of course, in a real fan, downstream radiated power must pass through a stator blade row and is subject to modification.

Figures 7a and b compare compact source predictions with the noncompact calculations of Fig. 5 for upstream and downstream propagation, respectively. These figures indicate that the acoustic power differences between corresponding harmonics are considerable for the fundamental and third harmonic propagating upstream and for all harmonics propagating downstream, particularly in the range of θ_2 around the peak acoustic power generation.

An explanation for this behavior is as follows. The results in Fig. 7 correspond to summations over the inflow distortion circumferential mode number q. As q is varied, the noncompact acoustic power in the fundamental tone is sometimes higher and sometimes lower than that based upon the compact prediction (see Fig. 7 of Ref. 5). At large values of θ_2, the number of circumferential distortion harmonics which efficiently couple to propagating acoustic modes decreases, and the net acoustic power differences between noncompact and compact results are considerable and varied in magnitude. At small values of θ_2, the number of coupling distortion harmonics increases; therefore, the acoustic power differences among modes are averaged out to small net amounts in the summation over the wide range of coupled q's for a particular tone harmonic. The compact source predictions in Fig. 7 tend to underestimate the upstream acoustic power and overestimate downstream acoustic power in the fundamental tone. The trends at the second and third harmonics indicate that a compact source assumption underestimates harmonic power for both propagation directions. These results differ from those of Ref. 9, which considered only trends associated with single sinusoidal modes of inflow distortion entering a two-dimensional cascade. The summation over many distortion modes representing more complex shapes, such as the Gaussian, makes the effects of neglecting noncompactness specific to the particular case considered.

Figures 8a and b show the variation of the acoustic mode structure with the half-width of the Gaussian profile θ_2. Note that the minimum power calculated was -70 dB and that lower values are plotted at -70 dB. The step radial tip distortion assumed favors first radial mode generation similar to the results discussed in connection with Fig. 3. For particular modes, clear generation minima are also evident; e.g., for $\theta_2 = 0.0125$, $\ell = 0$, and $n = 2$ in Fig. 8a. The envelopes of the peak powers of the individual modes follow the trends with q shown in Fig. 6.

Comparisons of Theory and Experiment

A Single Tube Wake Interacting with a Rotor

Experiments were conducted in an anechoic wind tunnel[10] in which the variation of upstream radiated fundamental tone power was measured as a function of the length of a cylindrical-probe tube inserted through the inlet wall upstream of rotor 2. The wind tunnel was operated with 40 knots velocity, and the fan fundamental tone due to rotor-stator interaction was cut off such that inlet tone noise was dominated by the probe tube wake interacting with the rotor. Figure 9 shows the measured and calculated tone power (referenced to full immersion) as a function of probe immersion. The detailed shape of the probe tip is illustrated in the upper right corner of Fig. 9. The probe tube wake was modeled with Eqs. (9-11) as having a Gaussian profile in the circumferential direction. A step profile corresponding to immersion length was used to represent the radial distortion variation. The theoretical results show good agreement with the measured increases in fundamental tone power per length increment of probe im-

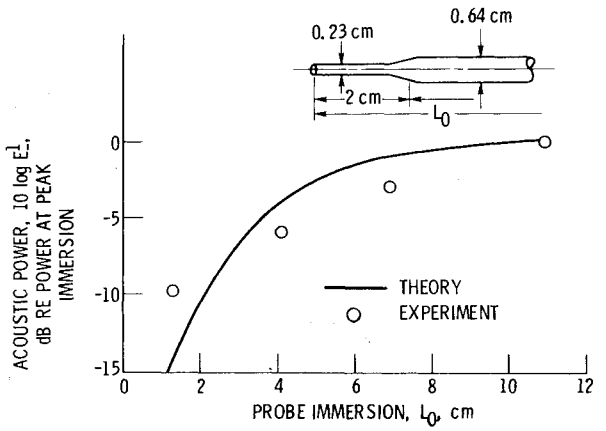

Fig. 9 Fundamental tone acoustic power generated by rotor-probe tube wake interaction, fan 2, upstream propagation, $C_D = 1.2$, $x^* = 27$ cm.

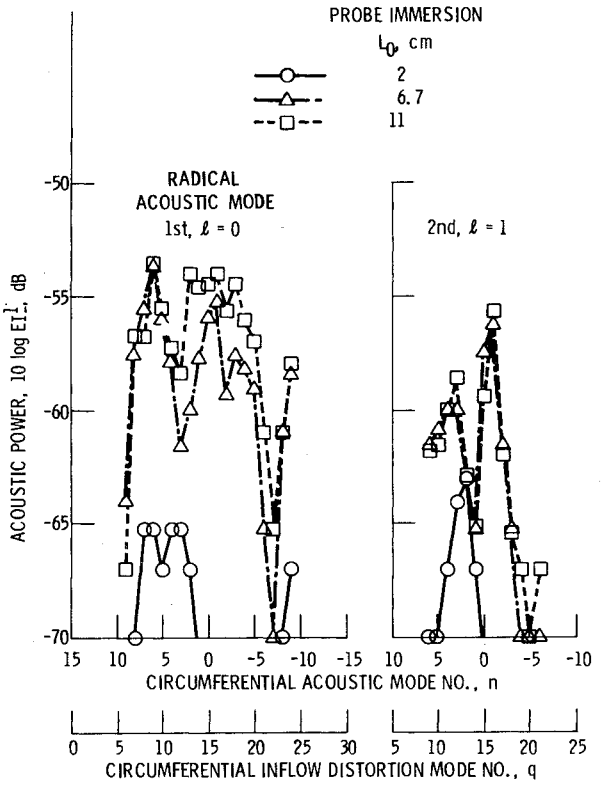

Fig. 10 Variation of fundamental tone modal structure with probe length immersed in a fan inlet, fan 2, upstream propagation.

mersion. For full immersion, $L_0 = 11$ cm, the calculated tone power is 130 dB compared with the measured value of 133 dB. The absolute amplitude calculated is subject to some uncertainty associated with the wake modeling, e.g., the effective θ_2 used to represent the complex probe tip. The absolute amplitude measured is also subject to uncertainty due to the probable asymmetric far-field radiation pattern associated with the single probe wake disturbance. However, the measurements were made in a plane coinciding within 5 deg of the plane through the probe and fan axes; therefore, the measured trend in power level with probe immersion is expected to be correct although the absolute levels might be too high. Of more significance is the agreement in the measured power trend with increasing probe immersion.

Figure 10 shows the variation of acoustic mode powers contributing to the fundamental tone as a function of probe tube immersion. The differences in mode power between 6.7- and 11-cm immersion are seen to be small for both the first and second radial modes, echoing the overall power variation shown in Fig. 9 and emphasizing that the generated power is dominated by the fan tip region, as previously shown in Ref. 5.

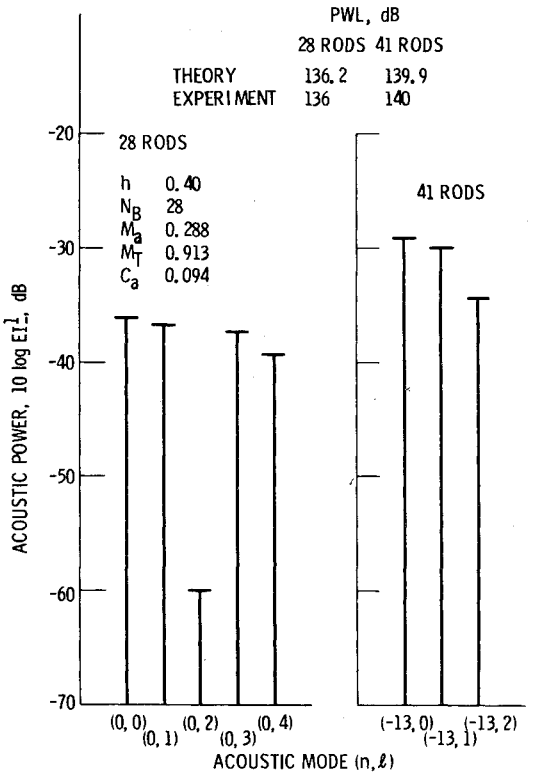

Fig. 11 Modal structure of the fundamental pure tone power generated by rod wakes interacting with a fan, fan 3, upstream propagation, $C_D = 1.2$.

Table 1 Fan parameters

	Fan 1	Fan 2	Fan 3
Rotor blade number, N_B	40	15	28
Dimensionless axial tip chord length, C_a	0.055	0.258	0.094
Rotor tip speed/axial flow speed, ω_T	2.474	1.052	3.011
Rotor relative Mach number, M_T	0.934	0.865	0.913
Axial flow Mach number, M_a	0.350	0.596	0.288
Hub/tip ratio, h	0.40	0.46	0.40

Multiple Rod Wakes Interacting with a Rotor

A JT15D turbofan engine was operated on an outdoor test stand with two separate sets of distortion rods (28 and 41) as a means of studying the transmission characteristics of inflow control devices.[11] The inflow control greatly reduced fan sources associated with inflow disturbances and left the dominant rod wake-rotor interaction as the main source of inlet noise. The fan parameters and operating condition are described in Table 1 as fan 3. The 28 rods were 0.635 cm in diameter and extended from the wall to 57.8% of the blade span, and the 41 rods were 0.476 cm in diameter and extended from the wall to 62.5% span. The centerline of both rod sets was located 8.9 cm upstream of the rotor tip. Figure 11 compares the calculated and measured fundamental tone power and shows the calculated distribution of modal powers for the two cases. The modal powers are roughly equal for the 28-rod case with the exception of the low third radial which

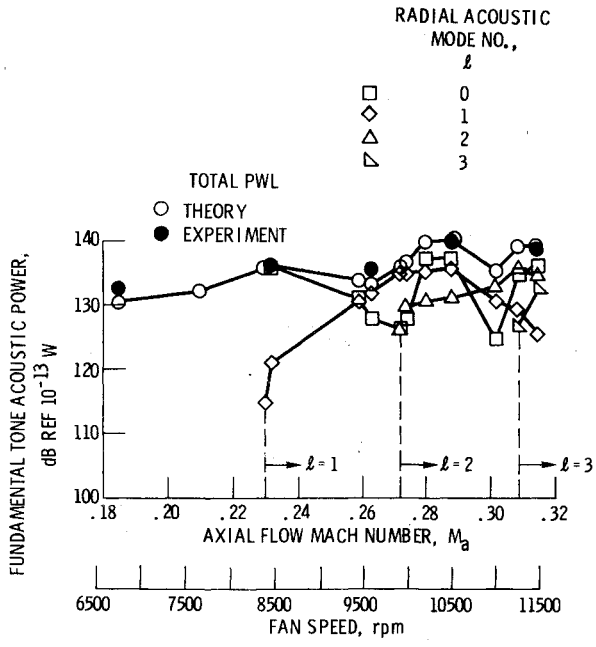

Fig. 12 Fan speed dependence of fundamental pure tone modal power generated by 41 rod wakes interacting with a fan, fan 3, upstream propagation.

appears to be another example of weak coupling between blade dipoles and the (0,2) acoustic mode. The agreement between measured and calculated tone power is excellent in each case, but such agreements of isolated powers are subject to some skepticism.

Figure 12 compares the measured and calculated fundamental tone powers as a function of fan speed for the 41-rod case. Calculated values of individual mode powers are also shown along with the speeds at which the individual radial modes begin to propagate. Agreement between calculated and measured tone levels is excellent over the entire speed range. Note that the power increase is not monotonic in either prediction or measurement and that the radial mode mix contributing to the total power changes from speed to speed. Minimum mode power occurs at "cut-on."

The ultimate comparison of interest is between measured and calculated far-field directivities. However, several links in the analytical chain relating source modes in an annulus to far-field directivity are missing. The modal scattering in the transition from an annular to a circular duct awaits detailed numerical solution as does the detailed radiation from an unflanged inlet duct to the far-field with a superimposed inlet potential flow field. Reference 12 looks at this same rod disturbance data from the standpoint of inferring source modal content from the far-field directivity. A reconciliation of those results with the present calculation requires additional analysis.

Concluding Remarks

The three-dimensional, noncompact source theory has been applied to calculate fan tone power and detailed acoustic mode structure for several assumed inflow distortions of increasing complexity and for experimental situations where upstream radial rods generated the distortions. While generated radial acoustic mode structure can be rationalized for tip distortions (first radial distortion modes appear to favor first radial acoustic modes), the radial acoustic mode content becomes much more complex for higher-order radial distortion modes. Circumferential distortion profiles such as the Gaussian used herein simply generate circumferential acoustic mode content corresponding to the circumferential Fourier harmonic content of the distortion. However, individual acoustic mode levels are subject to a coupling constraint associated with the way the dipoles on the blade surfaces couple to a particular acoustic mode. Poor coupling results in very low values of generated mode power. The use of this minimum generation property to practically reduce fan noise would require that the mode minimized be the sole mode responsible for the particular tone harmonic power generation at the given fan operating condition. The presence of other modes not obeying the particular decoupling constraint would defeat the tone power minimization. Generalizations regarding the magnitude and sign of the differences between the compact and the noncompact source results are not available for complex inflow distortions since the net tone powers are the result of summations over many individual modes, each having varied degrees of noncompact dependence. The fact that the analysis is able to predict the trend in tone power as a function of the immersion depth of an upstream rod disturbance and the variation of tone power with fan speed for multiple rod wake disturbances is encouraging. An important task remaining is to link acoustic mode content at the fan face to far-field directivity patterns which can be compared with experimental results.

References

[1] Feiler, C. E. and Groeneweg, J. F., "Summary of Forward Velocity Effects on Fan Noise," AIAA Paper 77-1319, Oct. 1977.

[2] Saule, A. V. and Rice, E. J., "Far-Field Multi-Modal Acoustic Radiation Directivity," NASA TM-73839, Dec. 1977.

[3] Rice, E. J., Heidmann, M. F., and Sofrin, T. G., "Modal Propagation Angles in a Cylindrical Duct with Flow and Their Relation to Sound Radiation," NASA TM-79030, Jan. 1979.

[4] Rice, E. J., "Spinning Mode Sound Propagation in Ducts with Acoustic Treatment," NASA TN D-7913, May 1975.

[5] Kobayashi, H., "Three-Dimensional Effects on Pure Tone Fan Noise Due to Inflow Distortion," AIAA Paper 78-1120, Seattle, Wash., July 1978.

[6] Namba, M., "Three-Dimensional Analysis of Blade Force and Sound Generation for an Annular Cascade in Distorted Flows," *Journal of Sound and Vibration*, Vol. 50, Feb. 1977, pp. 479-508.

[7] Schlichting, H., *Boundary-Layer Theory*, 6th Ed., McGraw-Hill, New York, 1968.

[8] Pickett, G. F., "Effects of Nonuniform Inflow on Fan Noise," *Journal of Acoustical Society of America*, Vol. 55, Suppl., Session B5 April 1974, Abstract, p. S4.

[9] Kaji, S., "Noncompact Source Effect on the Prediction of Tone Noise from a Fan Rotor," AIAA Paper 75-446, Hampton, Va., March 1975.

[10] Shaw, L. M., Woodward, R. P., Glaser, F. W., and Dastoli, B. J., "Inlet Turbulence and Fan Noise Measured in an Anechoic Wind Tunnel and Statically with an Inlet Flow Control Device," AIAA Paper 77-1345, Atlanta, Ga., Oct. 1977; also published as NASA TM-73723.

[11] Jones, W. L., McArdle, J. G., and Homyak, L., "Evaluation of Two Inflow Control Devices for Flight Simulation of Fan Noise Using a JT15D Engine," AIAA Paper 79-0654, Seattle, Wash., March 1979.

[12] Heidmann, M. F., Saule, A. V., and McArdle, J. G., "Analysis of Radiation Patterns of Interaction Tones Generated by Inlet Rods in the JT15D Engine," AIAA Paper 79-0581, Seattle, Wash., March 1979.